Progress In Electromagnetics Research, Vol. 122, 497–518, 2012

IMPROVING THE RELIABILITY OF FREQUENCY DOMAIN SIMULATORS IN THE PRESENCE OF HOMOGENEOUS METAMATERIALS — A PRELIMINARY NUMERICAL ASSESSMENT

G. Oliveri*

ELEDIA Research Center, Department of Information Engineering and Computer Science, University of Trento, Via Sommarive 14, Trento 38123, Italy

Abstract—The accuracy of the finite difference frequency domain (*FDFD*) method in the solution of canonical waveguide discontinuity problems involving complementary or nearly complementary metamaterials (*MTM*s) is analytically discussed. It is shown that the good accuracy of the method (in comparison with other frequency-domain techniques) is due to the intrinsic approximation which it introduces in the finite-difference discretization of sharp dielectric interfaces. By exploiting such a result, a perturbation algorithm is proposed for the reliable modeling of *MTM*s devices when other frequency domain numerical methods are at disposal. A preliminary numerical analysis is carried out to assess the reliability and accuracy of the proposed modeling approach when canonical scattering problems are at hand.

1. INTRODUCTION AND RATIONALE

In the recent years, there has been an explosive activity at the research and industrial level [1, 2] in the development and testing of metamaterials (*MTM*s), as it is demonstrated by the the large number of contributions on theoretical [3–8] as well as practical [9–15] aspects of this emerging field. Such an extraordinary interest is actually motivated by the unique capabilities of these artificial materials to modify the propagation characteristics of electromagnetic waves [1, 2], which allows the design of innovative applications which were never before thought possible.

Received 8 October 2011, Accepted 25 November 2011, Scheduled 8 December 2011

* Corresponding author: Giacomo Oliveri (giacomo.oliveri@disi.unitn.it).

Metamaterials usually consist of periodic arrangements of dielectric/metallic particles embedded in host regions, and their effective (i.e., homogeneous) responses are tailored from the geometry of their constituents rather than from their chemical properties [16, 17]. Moreover, metamaterials are also normally characterized not only by frequency dispersion but also by strong spatial dispersion, i.e., their effective permittivities depend not only on frequency but also the wave vector [16, 17]. Accordingly, homogenization represents a challenging topic in metamaterial science, as demonstrated by the serious research efforts carried out in this area [16, 17].

In this framework, numerical techniques able to reliably simulating complex devices based on homogeneous *MTM*s are becoming increasingly important [18–20]. This is particularly true for the simulations carried out at the early stages of the design process, when these materials are usually characterized at the macroscopic level [8, 12]. Indeed, it is a common approach to take into account the fine *MTM* structures only after the initial design has been completed and optimized [18]. Accordingly, the success of *MTM*s has led to a growing interest in numerical methods able to reliably treat "effective" *MTM*s [18, 19].

In this framework, surprisingly poor performances have been recently obtained by some widely used techniques [e.g., the finite element (*FE*) method [21]] when simulating canonical waveguide and scattering problems involving *MTM*s [22, 23]. Moreover, some theoretical analyses of problems involving metamaterials have shown that simple frequency-domain waveguide discontinuity problems can be ill-posed [24] even in the presence of lossy media and of absorbing boundary conditions [23]. From a numerical viewpoint, such anomalies have shown to cause a strong numerical instability for the *FE* method, especially in configurations involving interfaces with "complementary" or nearly complementary media [22, 23]. Such results have been demonstrated even using a commercial simulator with problems which are believed to be well-posed [25].

More recently, the effects of *MTM*s on other numerical techniques has been considered, and the first results regarding a waveguide discontinuity problem solved by a simple finite-difference frequency-domain (*FDFD*) method have been reported [26, 27]. Such results have shown that the *FDFD* technique yields a significantly higher accuracy in the solution of problems involving *MTM*s, even if the most "critical" configurations are considered [26]. However, to the best of the authors' knowledge, no clear explanation of such results has been provided yet.

The paper has a twofold objective. On the one hand, it is aimed at deducing the theoretical motivations for the good results obtained

by the *FDFD* method when dealing with metamaterials. Towards this end, a transmission-matrix approach is deployed to analyze the "effective" model actually solved by the *FDFD* technique (as well as by other related methods, such as the finite integration technique [28] and the finite-difference time-domain method [29]) when *MTM* waveguides are at hand. On the other hand, it is devoted to exploiting such an explanation to heuristically deduce a perturbation algorithm which improves the accuracy of other frequency domain numerical methods (such as the *FE* method) when dealing with *MTM*s. Accordingly, the proposed stabilization algorithm is preliminary numerically validated (by exploiting a commercial *FE* solver [30]) against a wide set of electromagnetic problems belonging to two canonical classes: a waveguide discontinuity problem, and a multi-layer sphere scattering problems.

The paper is organized as follows. Previous results obtained in the modeling of *MTM* through widely known numerical methods are firstly resumed (Section 2), specifically focusing on the high reliability of the *FDFD* method, which is then theoretically analyzed (Section 3). Afterwards, the improved *MTM* modeling algorithm is proposed (Section 4) and numerically validated (Section 5). Finally, some conclusions are drawn (Section 6).

2. MATHEMATICAL FORMULATION AND PREVIOUS RESULTS ON *FE* AND *FDFD* MODELING OF *MTM*S

Let us consider a canonical rectangular waveguide problem (whose analytical solution is easily computable) characterized by an aperture

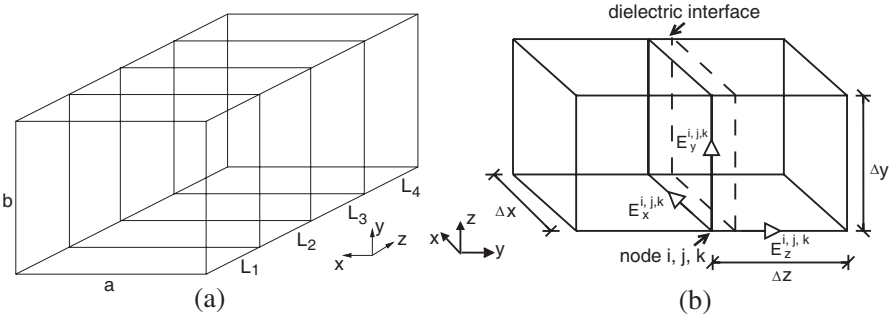

Figure 1. (a) Geometry of the waveguide discontinuity problem. (b) Discretization of the plane dielectric interface in the Yee grid, where only two 'cells' belonging to the E-grid are reported, along with the electric field component for the i-j-k-node.

$a \times b$ [along x and y, respectively — Fig. 1(a)] with perfect electric conductor (PEC) walls [26]. Along the z direction, the waveguide is subdivided into four homogeneous regions Ω_i of respective lengths $L_i\,(i = 1, \ldots, 4)$ characterized by a relative dielectric permittivity and magnetic permeability ε_i, $\mu_i\,(i = 1, \ldots, 4)$. Moreover, (possibly inhomogeneous) impedance boundary conditions are enforced on the two ports (at $z = 0$ and at $z = z_L = \sum_{i=0}^{4} L_i$).

To numerically solve such problem, the Maxwell equations

$$\begin{cases} \nabla \times \mathbf{E}(\mathbf{r}) = k_0 \bar{\bar{\mu}}_r(\mathbf{r}) \hat{\mathbf{H}}(\mathbf{r}) - \mathbf{J}_m(\mathbf{r}) \\ \nabla \times \hat{\mathbf{H}}(\mathbf{r}) = k_0 \bar{\bar{\varepsilon}}_r(\mathbf{r}) \mathbf{E}(\mathbf{r}) - j\eta_0 \mathbf{J}_e(\mathbf{r}) \end{cases} \tag{1}$$

must be discretized, where $\bar{\bar{\varepsilon}}_r(\mathbf{r})$ and $\bar{\bar{\mu}}_r(\mathbf{r})$ are the diagonal tensors of the relative dielectric permittivity and relative magnetic permeability, ε_0 and μ_0 are the free-space permittivity and permeability, $\eta_0 = \sqrt{\mu_0/\varepsilon_0}$, $k_0 = \omega\sqrt{\varepsilon_0\mu_0}$, ω is the angular frequency, $\hat{\mathbf{H}}(\mathbf{r}) = -j\eta_0 \mathbf{H}(\mathbf{r})$, $\mathbf{E}(\mathbf{r})$ and $\mathbf{H}(\mathbf{r})$ are the electric and magnetic fields, and $\mathbf{J}_e(\mathbf{r})$ and $\mathbf{J}_m(\mathbf{r})$ are the electric and magnetic current densities.

Unfortunately, the (very simple) described problem turns out ill-posed if Ω_2 and Ω_3 are composed of exactly complementary media, because its (unique) solution does not depend continuously on the data [23]. Indeed, it has been recently demonstrated that waveguide discontinuity problems can become ill-posed even in the presence of lossy media and absorbing boundary conditions [23]. Consequently, several anomalies of the numerical reliability of existing numerical methods, such as the *FE*3, have been pointed out in canonical direct scattering problems involving effective *MTM*s [22, 25, 31].

However, the *FE* instabilities have been confirmed even when the corresponding continuous problem is well-posed. In particular, the presence of complementary or almost complementary *MTM*s has shown to deeply affect the accuracy of the *FE* solutions and the convergence rate of some popular iterative solver used for the solution of the associated linear systems [22, 25, 31]. Accordingly, such preliminary conclusions [22, 25, 31] have suggested that *FE* method could have some intrinsic characteristics which make it particularly sensitive to the anomalies of *MTM* models.

To evaluate such possibility, a simple *FDFD* method has been exploited in [26] for the solution of problems involving *MTM*s similar to those defined in [23] [Fig. 1(a)]. In the *FDFD* approach, Eq. (1) is discretized in the domain of size $a \times b \times z_L$ by using a Yee grid [29, 32] composed of $N_x \times N_y \times N_z$ nodes in the x, y and z directions, respectively [26]. Accordingly, the following discretized curl equation

[first term in (1)] is introduced for the i, j, k *FDFD*-cell

$$-k_0\mu_{r,xx}^{i,j,k}\hat{H}_x^{i,j,k}+\left[E_y^{i,j,k}-E_y^{i,j,k+1}\right]/\Delta z+\left[E_z^{i,j+1,k}-E_z^{i,j,k}\right]/\Delta y=-J_{m,x}^{i,j,k} \quad (2)$$

$$-k_0\mu_{r,yy}^{i,j,k}\hat{H}_y^{i,j,k}+\left[E_x^{i,j,k+1}-E_x^{i,j,k}\right]/\Delta z+\left[E_z^{i,j,k}-E_z^{i+1,j,k}\right]/\Delta x=-J_{m,y}^{i,j,k} \quad (3)$$

$$-k_0\mu_{r,zz}^{i,j,k}\hat{H}_z^{i,j,k}+\left[E_y^{i+1,j,k})-E_y^{i,j,k}\right]/\Delta x+ \quad (4)$$

$$\left[E_x^{i,j,k})-E_x^{i,j+1,k}\right]/\Delta y=-J_{m,z}^{i,j,k} \quad (5)$$

where $\Delta x = \frac{D_x}{N_x-1}$, $\Delta y = \frac{D_y}{N_y-1}$, $\Delta z = \frac{D_z}{N_z-1}$ are the domain discretization steps, $\mu_{r,xx}^{i,j,k}$, $\mu_{r,yy}^{i,j,k}$, $\mu_{r,zz}^{i,j,k}$ are the relative dielectric parameters for the i, j, k cell, and the field components in the cell i, j, k are defined as

$$E_x^{i,j,k} = E_x(x_0+(i+0.5)\Delta x, y_0+j\Delta y, z_0+k\Delta z) \quad (6)$$

$$E_y^{i,j,k} = E_y(x_0+i\Delta x, y_0+(j+0.5)\Delta y, z_0+k\Delta z) \quad (7)$$

$$E_z^{i,j,k} = E_z(x_0+i\Delta x, y_0+j\Delta y, z_0+(k+0.5)\Delta z) \quad (8)$$

$$\hat{H}_x^{i,j,k} = \hat{H}_x(x_0+i\Delta x, y_0+(j+0.5)\Delta y, z_0+(k+0.5)\Delta z) \quad (9)$$

$$\hat{H}_y^{i,j,k} = \hat{H}_y(x_0+(i+0.5)\Delta x, y_0+j\Delta y, z_0+(k+0.5)\Delta z) \quad (10)$$

$$\hat{H}_z^{i,j,k} = \hat{H}_z(x_0+(i+0.5)\Delta x, y_0+(j+0.5)\Delta y, z_0+k\Delta z) \quad (11)$$

where it has been assumed that the domain of interest has the node $i = 0$, $j = 0$, $k = 0$ in (x_0, y_0, z_0) position [an analogous set of equations could be obtained from the other curl equation in (1)]. Quite surprisingly, the results obtained in [26] show that the considered *FDFD* method seems to find the solutions even to the above formulated ill-posed problems (i.e., when the media in Ω_2 and Ω_3 are complementary). However, only a qualitative explanation of such results have been provided so far [26].

3. AN EXPLANATION FOR THE *FDFD* ACCURACY WITH HOMOGENEOUS *MTM*S

3.1. *FDFD* Discretization of Sharp Interfaces

To fully explain the results in [26], the employed *FDFD* method is considered in more detail. Generally speaking, it is known that in *FDFD* (and *FDFD*) methods the assignment of the material properties to the grid cells (e.g., $\mu_{r,xx}^{i,j,k}$) is a fundamental step which can be performed by various techniques [29, 33, 34]. In [26], the pointwise value of the constitutive parameters has been assigned to each node

in the Yee grid (i.e., $\mu_{r,xx}^{i,j,k} = \mu_{r,xx}(i\Delta x, (j+0.5)\Delta y, (k+0.5)\Delta z)$, for example), and the discretization grid has been chosen in order to avoid that any node could lay on a discontinuity of the dielectric permittivity or of the magnetic permeability [26]. By observing Eqs. (2)–(4), it can be deduced that such a choice actually introduces a small but fundamental modification in the model numerically solved by the *FDFD*. Indeed, let us consider a plane dielectric interface along the z direction, and assume that the nodes of the Yee grid are placed as in Fig. 1(b). By considering Eq. (2) for instance, one can note that the *FDFD* method actually enforces a constant $\mu_{r,xx}$ for $x = x_i$, $y_j < y < y_{j+1}$, $z_k < z < z_{k+1}$, that is well beyond the end of the "true" media interface [see Fig. 1(b)]. Accordingly, the problem actually solved by the *FDFD* method turns out "modified" with respect to the ideal one [Fig. 2(a)], specifically because the discretization "creates" a transition layer (whose width is equal to around half the cell size, on the average) in correspondence of any dielectric interface in which both the permittivity and the permeability have different values [Fig. 2(b)]. Moreover, it could be easily demonstrated that such layer can even turn out anisotropic even if only isotropic media are considered in the problem.

Obviously, the perturbation caused by the *FDFD* discretization has an impact on the numerically computed solution (which necessarily differs from the analytical one), as well as on the properties of the corresponding model. To analyze if such perturbation is the responsible for the "problem" stabilization observed in [26], some assumption is mandatory. More specifically, if an isotropic transition

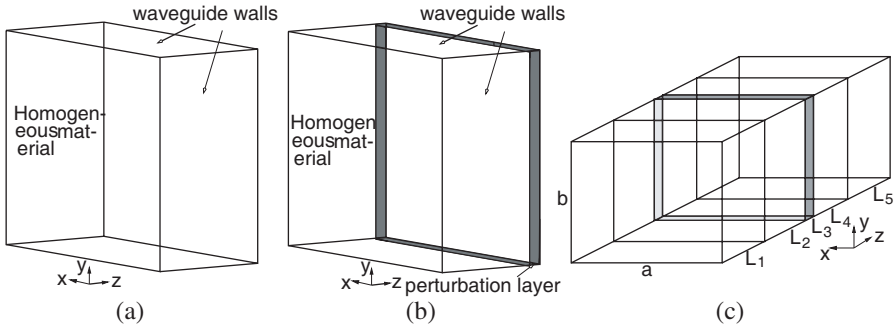

Figure 2. Simplified model for the perturbation introduced by the considered *FDFD* method in a problem of Class I. Only the central (gray) layer is introduced for simplicity. (a) Single slab in the original geometry. (b) Deduced perturbed slab. (c) Complete geometry of interest.

layer of thickness equal to $\Delta z/2$ is assumed to be introduced by the discretization process between Ω_2 and Ω_3 (i.e., in the transition between the complementary regions), the "perturbed" model actually solved instead turns out to consist of *five* homogeneous regions Ω_i^p of length $L_i^p\,(i = 1, \ldots, 5)$ with relative dielectric permittivity and relative magnetic permeability equal to ε_i^p, $\mu_i^p\,(i = 1, \ldots, 5)$ [Fig. 2(c)]. Due to the previous considerations, one can easily deduce that the perturbed model is characterized by $\varepsilon_1^p = \varepsilon_1$, $\mu_1^p = \mu_1$, $L_1^p = L_1$, $\varepsilon_2^p = \varepsilon_2$, $\mu_2^p = \mu_2$, $L_2^p = L_2 - \Delta z/4$, $\varepsilon_3^p = \varepsilon_2$, $\mu_3^p = \mu_2$, $L_3^p = \Delta z/2$, $\varepsilon_4^p = \varepsilon_3$, $\mu_4^p = \mu_3$, $L_4^p = L_3 - \Delta z/4$, $\varepsilon_5^p = \varepsilon_4$, $\mu_5^p = \mu_4$, and $L_5^p = L_4$. According to the above assumptions, an isotropic single negative (SNG) layer of thickness $\Delta z/2$ is actually introduced by the *FDFD* discretization process [Fig. 2(c)]. However, essentially the same results would be obtained also by considering the most general case of anisotropic layers.

3.2. Analysis of *FDFD* Perturbation through a Transmission Matrix Approach

In order to analyze the property of the arising "perturbed" model, let us consider the *ABCD* (transmission) matrix methodology [35]. Such an approach significantly simplifies the solution of the considered problem as it reduces to the combination of the *ABCD* matrices of all slabs (Ω_i) [35], which can be easily evaluated.

Towards this end, let us start with the computation of the *ABCS* matrix for the m-th TE or TM mode in the waveguide in a single slab of thickness D characterized by the relative dielectric parameters ε_A, μ_A [see Fig. 2(a)], which is equal to

$$T^m = \begin{bmatrix} \cosh(\gamma_A^m D) & \eta_A^m \sinh(\gamma_A^m D) \\ \sinh(\gamma_A^m D)/\eta_A^m & \cosh(\gamma_A^m D) \end{bmatrix}. \tag{12}$$

Moreover, the transmission matrix for a perturbed slab [Fig. 2(b)] turns out equal to

$$T_p^m = \begin{bmatrix} \{\eta_B^m \cosh(\gamma_A^m(D-t)) & \eta_B^m \cosh(\gamma_A^m(D-t)) \\ \cosh(\gamma_B^m t) + \eta_A^m & \sinh(\gamma_B^m t) + \\ \sinh(\gamma_A^m(D-t)) & + \eta_A^m \sinh(\gamma_A^m(D-t)) \\ \sinh(\gamma_B^m t)\}/\eta_B^m & \cosh(\gamma_B^m t) \\ \dfrac{\sinh(\gamma_A^m(D-t))\cosh(\gamma_B^m t)}{\eta_A^m} + & \{\eta_B^m \sinh(\gamma_A^m(D-t)) \\ & \sinh(\gamma_B^m t) + \\ + \dfrac{\cosh(\gamma_A^m(D-t))\sinh(\gamma_B^m t)}{\eta_B^m} & + \eta_A^m \cosh(\gamma_A^m(D-t)) \\ & \cosh(\gamma_B^m t)\}/\eta_A^m \end{bmatrix} \tag{13}$$

where t is the thickness of the perturbation layer whose dielectric parameters are ε_B, μ_B [Fig. 2(b)], γ_A^m and η_A^m are, respectively, the propagation constant and the impedance of the TE or TM mode m in the original slab (γ_B^m and η_B^m represent the same quantities in the perturbation layer). It is important to remark that such expressions do not depend on the guiding structure or on the considered TE or TM mode, provided that the formalism of current and voltage waves can be used.

If $|\gamma_A^m t|$ and $|\gamma_B^m t|$ are small, Eq. (13) can be easily transformed into

$$T_p^m \approx T^m + T_{\text{err}}^m \tag{14}$$

where

$$T_{\text{err}}^m = t\gamma_A^m \begin{bmatrix} \Psi \sinh(\gamma_A^m D) & \Phi\eta_A^m \cosh(\gamma_A^m D) \\ \Psi \dfrac{\cosh(\gamma_A^m D)}{\eta_A^m} & \Phi \sinh(\gamma_A^m D) \end{bmatrix} \tag{15}$$

and $\Psi \triangleq (\frac{\gamma_B^m}{\gamma_A^m}\frac{\eta_A^m}{\eta_B^m} - 1)$, $\Phi \triangleq (\frac{\gamma_B^m}{\gamma_A^m}\frac{\eta_B^m}{\eta_A^m} - 1)$ (which are assumed to be different from zero). From (13)–(15), it can be deduced that the error introduced by the perturbation layer increases with the amplitude of the propagation constant of the considered mode, and that, as expected, it approaches zero as $t \to 0$.

Several conclusions can be drawn from the above results. Indeed, if we now take Eqs. (14) and (15) as the equations describing the *ABCD* matrices of the SNG layer introduced by the *FDFD*, it turns out that the perturbation on the solution due to the *FDFD* discretization actually approaches zero as its thickness t goes to zero, as expected. However, whatever the $t \neq 0$, the perturbation is small only for a certain number (depending on the angular frequency ω) of lower modes, while it becomes more and more significant for the upper modes (possibly below cutoff).

Such a result has a fundamental importance in terms of the mathematical features of the arising problem. More specifically, the above conclusion means that the original and the perturbed model are not *equivalent.* Indeed, the ill-posedness of the original model is due to the existence of an infinite sequence of surface modes (below cutoff) around the interface [23]. Due to the introduced slab, such modes cannot exist in the perturbed problem. Accordingly, it is deduced that the effectiveness of the *FDFD* methodologies in the ill-posed class of problem of Fig. 1(a) is fundamentally caused by the modeling error it implicitly introduces during the discretization process. Of course, it must be pointed out that if the solution of interest is represented

by a superposition of a finite set of modes (as in [26]), it is always possible to find a t ($\Rightarrow \Delta z$) such that all the considered $ABCD$ matrices are affected by a perturbation which is below a desired threshold. Accordingly, it turns out that, by suitably selecting t, it is possible to (a) achieve a reliable solution for the original model, while (b) avoiding its ill posedness.

Furthermore, one can note that the perturbed solution is a good approximation of the original one if t is small, which means that Δz is small in the *FDFD* simulations. This is actually confirmed by the results reported in [26], where accurate solutions require a much finer discretization along the z axis than along the other axes.

4. THE PROPOSED *MTM* MODELING GUIDELINES

In the previous Section, it was shown that the application of the considered *FDFD* method implicitly introduces a perturbation (SNG layer) in the model. Such an implicit procedure improves the accuracy of the method with respect to other widely used techniques at the expenses of increased memory requirements due to the necessity of significantly reducing Δz (especially around the complementary interfaces).

It is quite straightforward to consider such a result from a different viewpoint. Indeed, one could ask if such kind of perturbation could be introduced in an explicit manner in the ill-posed waveguide problems, or on similar "critical" configurations (such as those considered in [25]), and then improve the performances of other frequency-domain numerical simulators[†]. It is worth pointing out that much more degrees of freedom would be available for the designer (with respect to the exploitation of the "implicit" *FDFD* processing). As a matter of fact, both the dielectric characteristics and thickness t of the "perturbation layer" could be easily modified according to the design targets.

According to the above considerations, the design of a "perturbation layer" to be introduced in the complementary or nearly complementary dielectric interfaces is proposed with the aim of improving the accuracy of frequency domain numerical methods. More in detail, because of the infeasibility of a general-purpose proof regarding the reliability of the deduced algorithm, an heuristic approach will be followed. In the derivation, the perturbation will be introduced on just one side of the "critical" interface (i.e., only the

[†] It is worth pointing out that transition layers are already employed in some versions of finite-difference algorithms [29]. However, their exploitation for the stabilization of other frequency-domain approaches when dealing with *MTM*s has never been considered so far, to the best of the author's knowledge.

DPS slab will be modified), for simplicity.

The most straightforward perturbation problem to be solved could be the following:

Problem 1 *given (ω) and the medium properties of the layer to be perturbed, find (t) and the dielectric properties of the perturbation layer such that the perturbation introduced on the (T^m) of interest (those corresponding to the modes which have to be approximated correctly) is below a given threshold.*

Which can be considered as an inverse problem where the dielectric characteristics of an unknown material have to be retrieved, as it is usually done in microwave imaging [36–38]. Of course, several different layers satisfy the objective of Algorithm 1: as an example, the trivial solution $t = 0$ would be certainly acceptable. However, it is important to observe that the introduced perturbation should be the maximum allowed by the given threshold, so that the actually solved model is sufficiently different from a "critical" configuration (i.e., presence in the problem of an almost complementary interface [25]). Moreover, it obvious to notice that a too thin t would require a very fine discretization around the interface (in order to obtain a good description of the model), which would obviously mean an increase in the memory requirements.

In order to simplify the calculations for the "optimal perturbation layer" while satisfying the above requirements, the following modified problem is then formulated.

Problem 2 *given ω and the medium properties of the layer to be perturbed, find the maximum t such that the linear approximation (14) holds true; then choose the media of the perturbation layer such that $||T^m_{\rm err}||_1$ is maximum, subject to a constraint on the perturbation introduced on the modes which have to be approximated correctly.*

It could be obviously possible to set up an optimization problem [36, 39, 40] from the analytical evaluation of $||T^m_{\rm err}||_1$ for the considered TE and/or TM modes. However, to simplify the arising algorithm, an additional approximation is performed. by assuming that

$$\gamma_i^m \approx \gamma_i^{\rm TEM} = j\omega\sqrt{\varepsilon_0\varepsilon_i\mu_0\mu_i} \tag{16}$$

$$\eta_i^m \approx \eta_i^{\rm TEM} = \frac{\mu_i\mu_0}{\varepsilon_i\varepsilon_0} \tag{17}$$

for the modes which have to be approximated accurately, where $i = A, B$, that is that the propagation constants and impedances of the modes of interest in the considered slab. By using the

approximations (16) and (17), it turns out that

$$\Psi = \frac{\varepsilon_B - \varepsilon_A}{\varepsilon_A} \tag{18}$$

$$\Phi = \frac{\mu_B - \mu_A}{\mu_A}. \tag{19}$$

Finally, by noticing that $||T^m_{\rm err}||_1$ directly depends on $|\Psi|$ and $|\Phi|$, the constraint on $||T^m_{\rm err}||_1$ can be turned into simpler ones on the expression in (18) and (19). The resulting (final) perturbation technique is the following.

Problem 3 *given ω and the medium properties of the layer to be perturbed, find the maximum t such that the linear approximation (14) holds true; then choose the media of the perturbation layer such that $|\Psi|$ and $|\Phi|$ are maximum, subject to $|\Psi| \leq C_\Psi$ and $|\Phi| \leq C_\Phi$.*

Where C_Ψ and C_Φ are real positive constants which depend on the accepted perturbation on the "desired" modes. By simple computation, it turns out that Problem 3 has the following solution

$$\begin{cases} t = \min\left\{\dfrac{C_t}{|\gamma_A|}, \dfrac{C_t}{|\gamma_B|}\right\} \\ \varepsilon_B = \varepsilon_A + C_\Psi|\varepsilon_A|e^{j\chi} \\ \mu_B = \mu_A + C_\Phi|\mu_A|e^{j\xi} \end{cases} \tag{20}$$

where C_t is a positive quantity which assures that the linear approximation (14) holds true, and χ and ξ are arbitrary phase terms. In the following, the degree of freedom in the choice of χ and ξ will be used to insert the maximum amount of losses in the perturbation layer (i.e., $\chi = \xi = -\frac{\pi}{2}$). Such choice is motivated by the already performed numerical analyses on the stability of numerical solvers in the presence of MTMs [22, 31, 25].

5. PRELIMINARY NUMERICAL RESULTS

This section is aimed at providing examples of the application of the above deduced guidelines, as well as at preliminary assessing their features when applied to more general scattering problems. Towards this end, Eq. (20) will be applied within a commercial *FE* solver based on an edge-element formulation [30], and the arising results will be compared to those achieved by the original method.

5.1. Canonical Waveguide Problem

The first numerical experiment deals with the solution of the "critical" waveguide problems already considered in [25] which is characterized

by $a = 2b = 0.02\,\mathrm{m}$, $\varepsilon_1 = \varepsilon_4 = \mu_1 = \mu_4 = 1.0 - j0.1$, $\varepsilon_2 = \mu_2 = 1.0$, $\mathrm{Re}\,(\varepsilon_3) \in \{-0.5, -0.75, \ldots, -2.0\}$, $\mathrm{Im}\,(\varepsilon_3) \in \{0, -0.01, -0.1\}$, $\mathrm{Re}\,(\mu_3) \in \{-0.5, -0.75, \ldots, -2.0\}$, $\mathrm{Im}\,(\mu_3) \in \{0, -0.01, -0.1\}$, and $L_i = 0.03\,\mathrm{m}$ (for $i = 1, \ldots, 4$). The two waveguide ports are matched to the propagation of the fundamental mode, and a unit amplitude TE_{10} mode at 11.25 GHz is impinging at $z = 0$.

By using (20), a perturbed problem is then defined for each original problem by setting $\varepsilon_B = \mu_B = 1.0 - j0.02$ for $z \in (0.059, 0.06)$ (that is $t = 0.001$, and $\varepsilon_A = \mu_A = \varepsilon_2 = \mu_2 = 1.0$). The numerical results are then compared with the analytical solution of the original (unperturbed) problem by computing the following error figure [25]

$$\eta = \frac{\int_\Omega \left| \frac{\mathbf{E}_{FE} - \mathbf{E}_{\mathrm{analytic}}}{\mathbf{E}_{\mathrm{analytic}}} \right| \mathrm{d}V}{\mathrm{volume}(\Omega)}, \tag{21}$$

where $\Omega = \{(x, y, z) \in \mathbb{R} | x \in (0, 0.02),\ y \in (0, 0.01),\ z \in (0.055, 0.065)\}$ is a subregion around the complementary interface, and $\mathbf{E}_{FE}$ and $\mathbf{E}_{\mathrm{analytic}}$ are the electric field calculated by the *FE* numerical simulator (for the perturbed problem) and analytically computed electric field, respectively. Two different discretizations have been considered during the simulations, corresponding to the "Normal" and "Fine" mesh settings of the solver.

The plots of the integral error η as a function of $\mathrm{Re}\,(\varepsilon_3)$ when $\mathrm{Im}(\varepsilon_3) = \mathrm{Im}(\mu_3) = 0$ and $\mathrm{Re}(\mu_3) = -1.0$ [Fig. 3(a)] indicate that the perturbation method yields a significant error reduction in the *FE* simulation whatever the considered discretization and permittivity of the Ω_3 region. Indeed, the error percentage for the "perturbed" models is always around or below 1%, thus showing a good accuracy for the direct solver [Fig. 3(a)]. On the contrary, the original discretized model yields errors up to five orders of magnitude higher [Fig. 3(a)]. Such a feature of *FE* simulation reveal the effectiveness of the proposed perturbation algorithm, which outperforms the original model in terms of accuracy even when using a coarser discretization (see perturbed model with "normal" mesh (blue line) vs. original model with "fine" mesh (green line) — Fig. 3(a)).

Similar results are obtained for larger and larger values of $\mathrm{Re}\,(\mu_3)$. Indeed, the plots of the integral errors in Figs. 3(b) and (c) confirm the significant enhancement allowed by the introduction of the thin slab according to (20) in the considered waveguide models. Indeed, the error reduces in the "original" model because the *DPS-DNG* interface is lesser and lesser "complementary" as $\mathrm{Re}\,(\mu_3)$ increases, but it still reaches values well above 30% (e.g., "normal" mesh, red line — Fig. 3(c). On the contrary, the perturbed model yields errors below 5% in all considered cases, (e.g., "normal" mesh, blue line — Fig. 3(c).

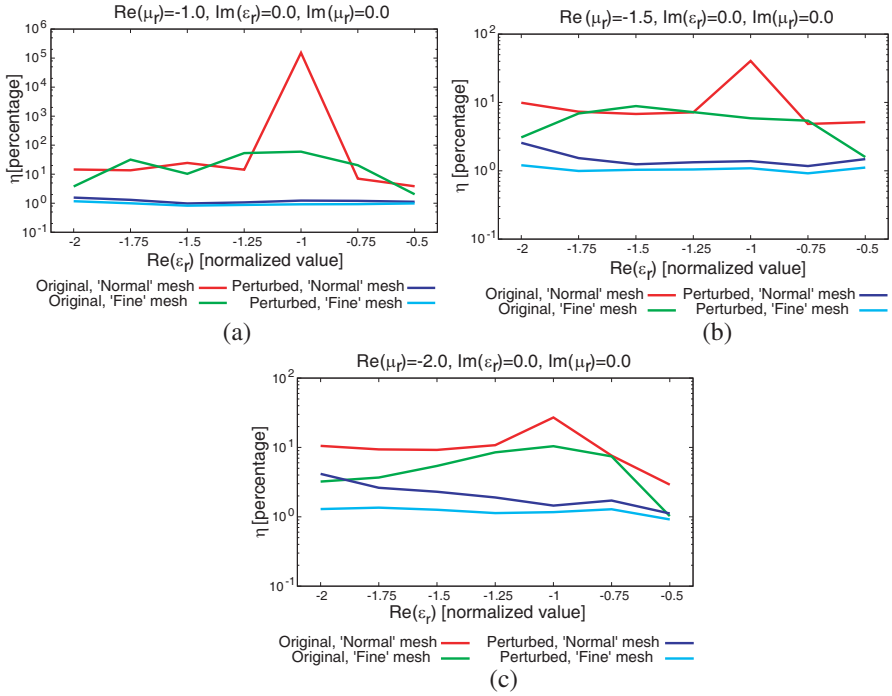

Figure 3. *Waveguide problem* [$\mathrm{Im}(\varepsilon_r) = \mathrm{Im}(\mu_r) = 0$] — Behaviour of η as a function of $\mathrm{Re}\,(\varepsilon_r)$ when (a) $\mathrm{Re}(\mu_r) = -1.0$. (b) $\mathrm{Re}(\mu_r) = -1.5$. (c) $\mathrm{Re}(\mu_r) = -2.0$.

Essentially the same results are obtained when considering the dependency of η on $\mathrm{Re}\,(\mu_3)$ (Fig. 4). Indeed, it can be easily noticed that the introduction of the thin slab significantly improves the method accuracy, both in the critical (i.e., complementary — Fig. 4(a)) as well as in close (Figs. 4(b), (c) configurations. Moreover, thanks to the considered perturbation, improved accuracy can be obtained even considering coarser meshes (e.g., blue line vs. green line in Fig. 4(a). Such a result points out that the proposed perturbation algorithm can also improve the computational efficiency of the considered frequency-domain numerical methods when dealing with *MTM*-enhanced devices.

As concerns lossy Ω_3 layers, it was noticed in [25] that the presence of non-negligible $\mathrm{Im}\,(\varepsilon_3)$ and/or $\mathrm{Im}\,(\mu_3)$ values can improve the stability of the *FE* approaches. To analyze the effectiveness and usefulness of the proposed perturbation approach in such a case, the same geometry was simulated taking into account larger and larger dielectric losses (Fig. 5 — "fine" mesh). As it can be noticed, the proposed perturbation algorithm still significantly enhance the

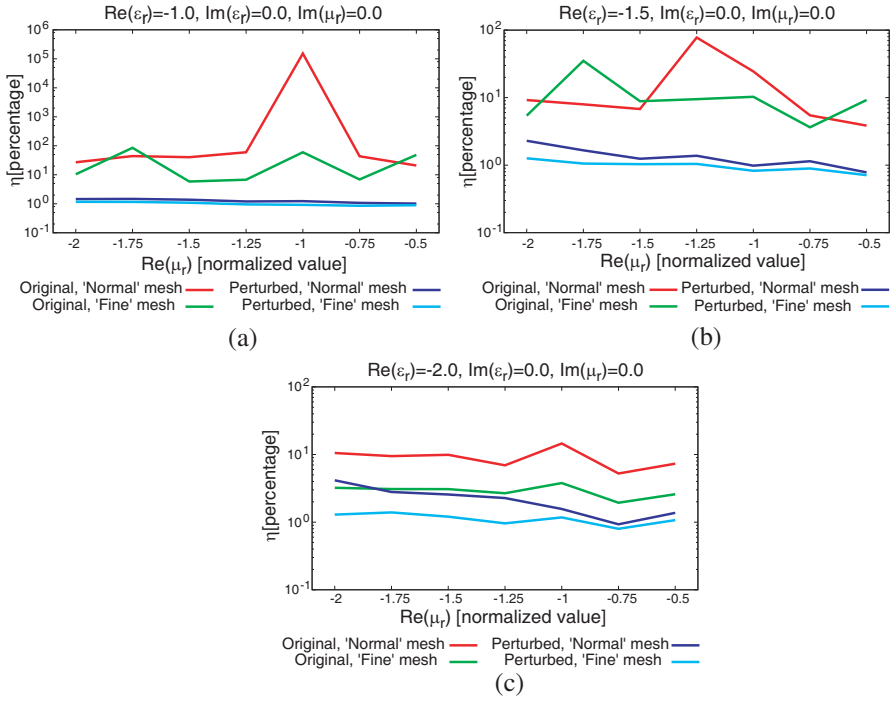

Figure 4. *Waveguide problem* [$\mathrm{Im}(\varepsilon_r) = \mathrm{Im}(\mu_r) = 0$] — Behaviour of η as a function of $\mathrm{Re}\,(\mu_r)$ when (a) $\mathrm{Re}(\varepsilon_r) = -1.0$. (b) $\mathrm{Re}(\varepsilon_r) = -1.5$. (c) $\mathrm{Re}(\varepsilon_r) = -2.0$.

accuracy of the commercial simulator (e.g., Fig. 5(a) vs. Fig. 5(b) — $\mathrm{Im}(\varepsilon_3) = \mathrm{Im}(\mu_3) = 0.01$), even when quite large losses are considered ($\mathrm{Im}(\varepsilon_3) = \mathrm{Im}(\mu_3) = 0.1$ — Fig. 5(c) vs. Fig. 5(d)). The performance improvement turns out even more evident when coarser discretization are at hand (Fig. 6 — "normal" mesh). These results further support the previous deductions regarding the enhancement allowed in terms of numerical efficiency as well as accuracy by the proposed perturbation algorithm.

5.2. Canonical Scattering Problem

To further assess the features and potentialities of the proposed algorithm, the simulation of the canonical scattering problem (homogeneous sphere) considered in [25] has been carried out either considering the original geometry or the perturbed one according to the criterion (20). More specifically, an original problem involving a *DNG* sphere of radius 0.2 m illuminated by a plane wave at 300 MHz and a

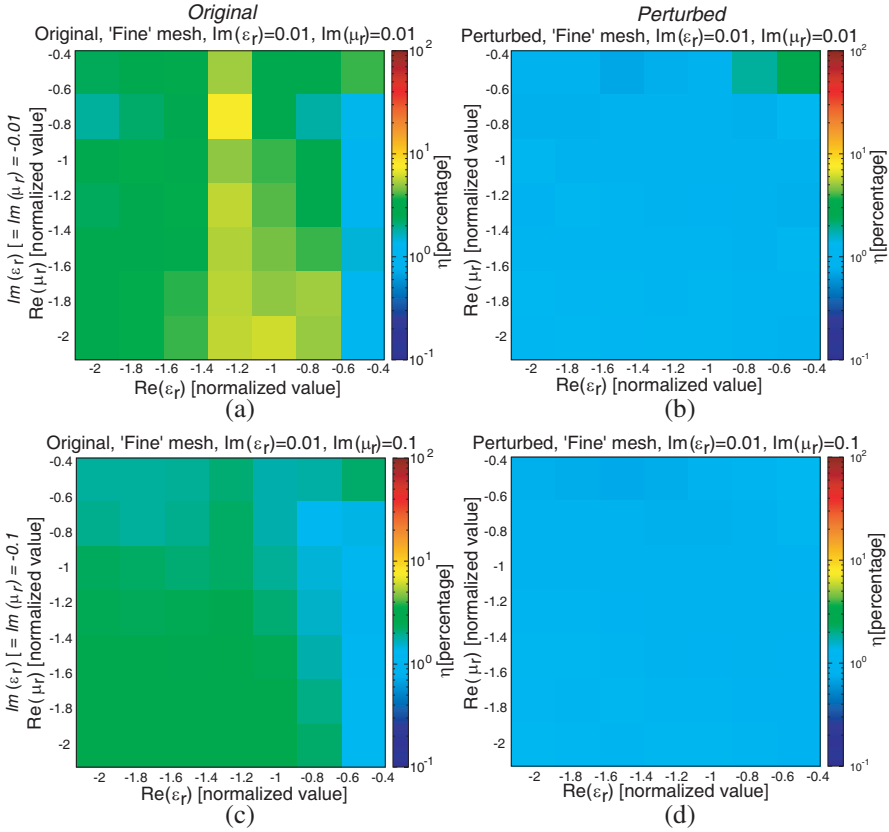

Figure 5. *Waveguide problem* [*"Fine" mesh*] — Behaviour of η as a function of $\mathrm{Re}\,(\varepsilon_r)$ and $\mathrm{Re}\,(\mu_r)$ when (a) (b) $\mathrm{Im}(\varepsilon_r) = \mathrm{Im}(\mu_r) = -0.01$ and (c) (d) $\mathrm{Im}(\varepsilon_r) = \mathrm{Im}(\mu_r) = -0.1$ for the (a) (c) *Original* or (b) (d) *Perturbed* models.

free-space cubic domain of size 1 m is considered for the simulations (whose analytical solution is known [25]), and it is perturbed by introducing a $t = 0.01$ m layer with relative dielectric parameters $\varepsilon_r = 1.0 - j0.02$, $\mu_r = 1.0$.

The plots of the total integral error η (computed assuming that Ω correspond to the entire investigation domain in this case) as a function of either $\mathrm{Re}\,(\varepsilon_{\mathrm{sphere}})$ (Figs. 7(a), (c), (e)) or $\mathrm{Re}\,(\mu_{\mathrm{sphere}})$ (Figs. 7(b), (d), (f)) reveal that the proposed perturbation algorithm turns out effective in terms of improved accuracy also in this scattering problem. Indeed, an error reduction factor up to almost two orders of magnitude can be achieved for the "normal" mesh, especially when "complementary" or "nearly complementary" interfaces are at

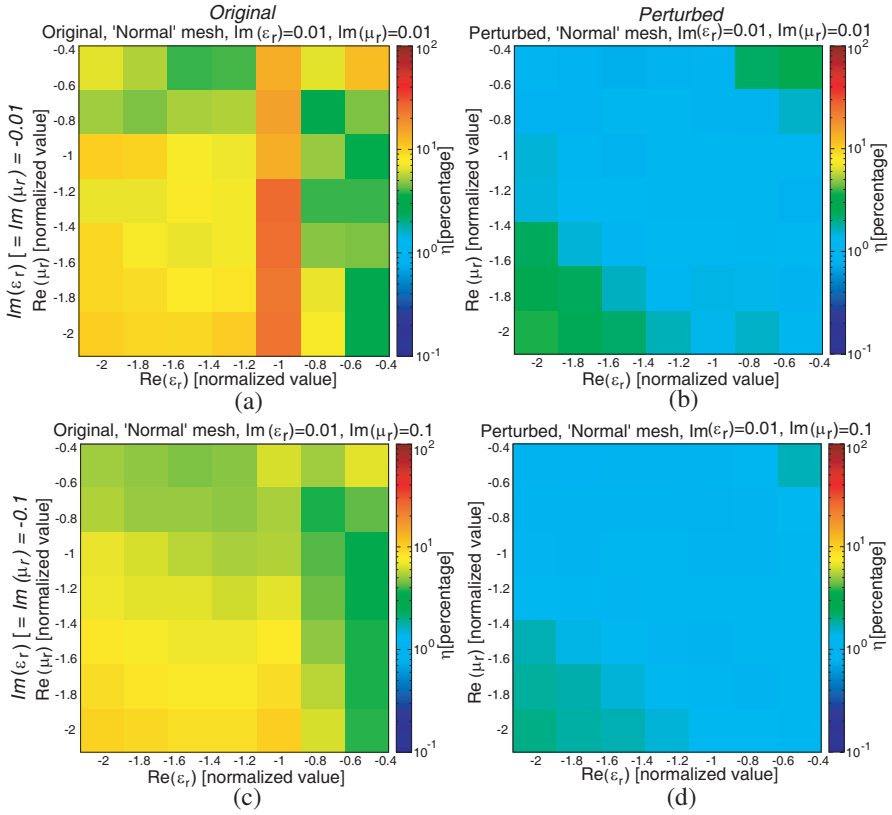

Figure 6. *Waveguide problem* [*"Normal" mesh*] — Behaviour of η as a function of $\mathrm{Re}\,(\varepsilon_r)$ and $\mathrm{Re}\,(\mu_r)$ when (a) (b) $\mathrm{Im}(\varepsilon_r) = \mathrm{Im}(\mu_r) = -0.01$ and (c) (d) $\mathrm{Im}(\varepsilon_r) = \mathrm{Im}(\mu_r) = -0.1$ for the (a) (c) *Original* or (b) (d) *Perturbed* models.

hand (Figs. 7(a), (b)). Moreover, the improvement is significant also when considering the "fine" discretization (e.g., Fig. 7(f)). It is also worth noticing that the enhancement allowed by the proposed perturbation layer allows the use of coarser meshes while achieving improved accuracies (e.g., blue line vs. green line in Fig. 7(d)), as it happened in the canonical waveguide case.

As a final experiment, the case of a lossy *DNG* sphere is considered to assess the potential advantages of the proposed modeling approach in this less critical scenario. Towards this end, the same scatterer geometry has been assumed setting $\mathrm{Im}(\varepsilon_{\mathrm{sphere}}) = \mathrm{Im}(\mu_{\mathrm{sphere}}) = -0.01$. By comparing the plots of the total integral error either for the "normal" (Figs. 8(a) vs. (b)) or the "fine" (Figs. 8(c) vs. (d))

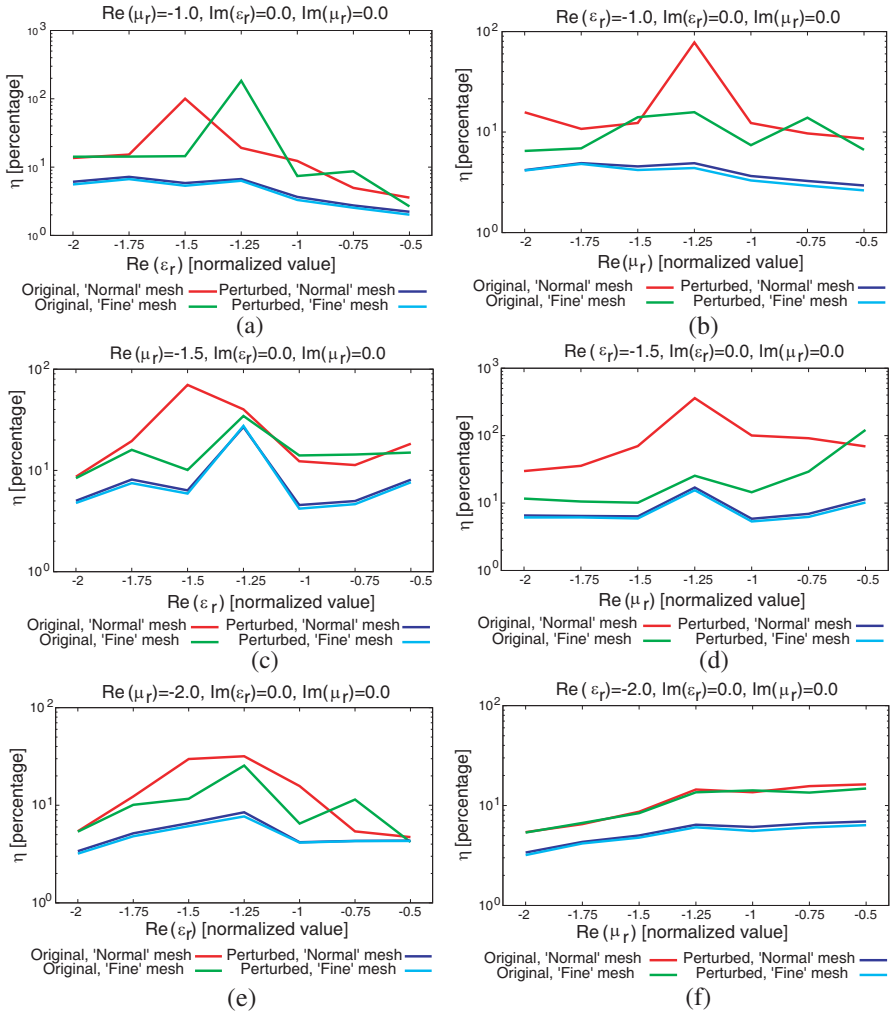

Figure 7. *Multilayer sphere problem* [$\mathrm{Im}(\varepsilon_r) = \mathrm{Im}(\mu_r) = 0$] — Behaviour of η as a function of (a) (c) (e) $\mathrm{Re}\,(\varepsilon_r)$ and (b) (d) (f) $\mathrm{Im}\,(\varepsilon_r)$ when (a) $\mathrm{Re}(\mu_r) = -1.0$. (c) $\mathrm{Re}(\mu_r) = -1.5$. (e) $\mathrm{Re}(\mu_r) = -2.0$. (b) $\mathrm{Re}(\mu_r) = -1.0$. (d) $\mathrm{Re}(\mu_r) = -1.5$. (f) $\mathrm{Re}(\mu_r) = -2.0$.

discretizations, it turns out that a significant improvement is allowed by the proposed perturbation algorithm also when lossy scatterers are of interest (e.g., Fig. 8(a) vs. Fig. 8(b)). Moreover, it is further remarked that the use of a thin perturbation layer can allow the use of coarser discretizations while achieving improved accuracies for the direct simulation(Fig. 8(b) vs. Fig. 8(c)).

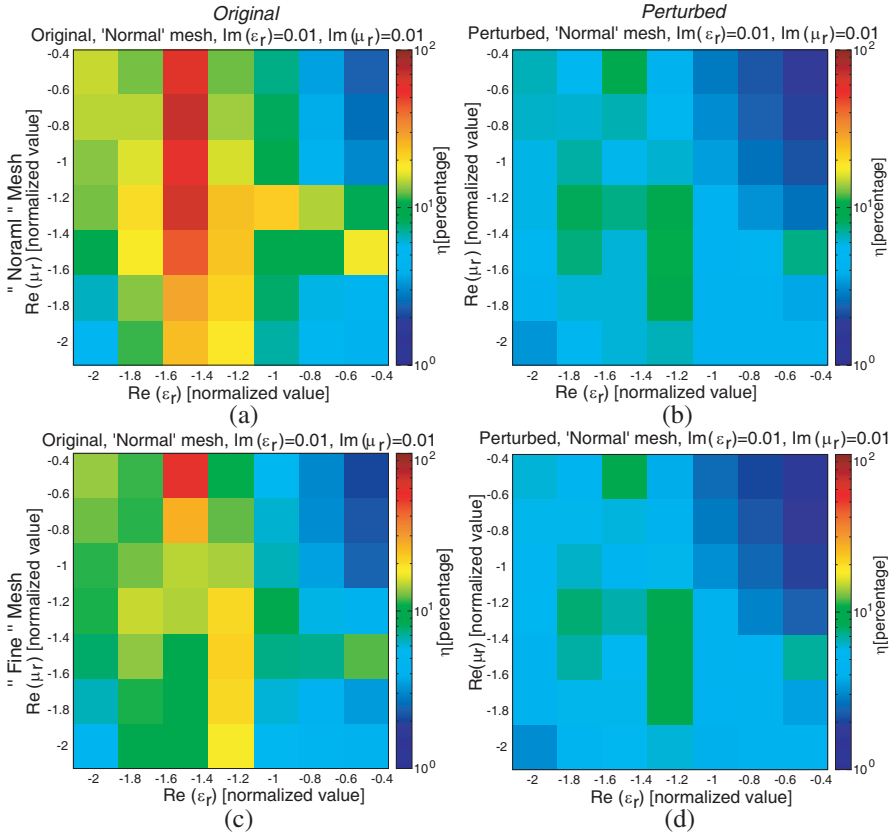

Figure 8. *Multilayer sphere problem* [$\mathrm{Im}(\varepsilon_r) = \mathrm{Im}(\mu_r) = -0.01$] — Behaviour of η as a function of $\mathrm{Re}\,(\varepsilon_r)$ and $\mathrm{Re}\,(\mu_r)$ when using (a) (b) "Normal" and (c) (d) "Fine" mesh settings with the (a) (c) *Original* or (b) (d) *Perturbed* models.

6. CONCLUSIONS AND REMARKS

A preliminary theoretical analysis of the accuracy of the *FDFD* in the solution of problems involving effective *MTM*s has been discussed. It has been deduced that a "transition layer" (sometimes employed in finite difference techniques) can suitably improve the stability of other numerical solvers when dealing with metamaterials. The provided motivation has been used to heuristically propose an innovative perturbation algorithm able to significantly improve the accuracy of frequency domain techniques, such as the *FE* method, when simulating devices which include effective metamaterials. Accordingly, the main contributions of the present work consist in the following

methodological novelties:

- the introduction of a simple closed-form explanation for the increased accuracy of finite-difference methods when dealing with *MTM*s (Section 3);
- the heuristic derivation of general purpose guidelines to be employed for the enhancement of the accuracy of arbitrary frequency-domain numerical simulators when dealing with homogeneous *MTM*s (Section 4).

The deduced algorithm has been tested on two canonical scattering problems by using a commercial *FE* simulator [30]. The numerical simulations have shown that, besides greatly improving the accuracy of the direct solver (Section 5), the proposed algorithm has shown the capability to reduce the memory required to perform effective simulations in the presence of *MTM*s (Fig. 8(b) vs. Fig. 8(c)).

Future works will be aimed at evaluating the performances of the proposed perturbation algorithm in *MTM* — enhanced devices with more complex geometries, as well as at deducing closed form solutions for the thickness and dielectric features of the perturbation layers when specific applicative problems are of interest.

REFERENCES

1. Ziolkowski, R. W. and N. Engheta, "Special issue on metamaterials," *IEEE Trans. on Antennas and Propag.*, Vol. 51, Oct. 2003.
2. Itoh, T. and A. A. Oliner, "Special issue on metamaterials structures, phenomena and applications," *IEEE Trans. on Microwave Theory and Tech.*, Vol. 53, Apr. 2005.
3. Canto, J. R., C. R. Paiva, and A. M. Barbosa, "Dispersion and losses in surface waveguides containing double negative or chiral metamaterials," *Progress In Electromagnetics Research*, Vol. 116, 409–423, 2011.
4. Chen, H., L. Huang, X. Cheng, and H. Wang, "Magnetic properties of metamaterial composed of closed rings," *Progress In Electromagnetics Research*, Vol. 115, 317–326, 2011.
5. He, Y., J.-Q. Shen, and S. He, "Consistent formalism for the momentum of electromagnetic waves in lossless dispersive metamaterials and the conservation of momentum," *Progress In Electromagnetics Research*, Vol. 116, 81–106, 2011.
6. Liu, L., J. Sun, X. Fu, J. Zhou, Q. Zhao, B. Fu, J. Liao, and D. Lippens, "Artificial magnetic properties of dielectric metamaterials in terms of effective circuit model," *Progress In Electromagnetics Research*, Vol. 116, 159–170, 2011.

7. Liu, S.-H. and L.-X. Guo, "Negative refraction in an anisotropic metamaterial with a rotation angle between the principal axis and the planar interface," *Progress In Electromagnetics Research*, Vol. 115, 243–257, 2011.
8. Valagiannopoulos, C. A., "Electromagnetic scattering of the field of a metamaterial slab antenna by an arbitrarily positioned cluster of metallic cylinders," *Progress In Electromagnetics Research*, Vol. 114, 51–66, 2011.
9. Feng, T., Y. Li, H. Jiang, W. Li, F. Yang, X. Dong, and H. Chen, "Tunable single-negative metamaterials based on microstrip transmission line with varactor diodes loading," *Progress In Electromagnetics Research*, Vol. 120, 35–50, 2011.
10. He, X.-J., Y. Wang, J. Wang, T. Gui, and Q. Wu, "Dual-band terahertz metamaterial absorber with polarization insensitivity and wide incident angle," *Progress In Electromagnetics Research*, Vol. 115, 381–397, 2011.
11. Shao, J., H. Zhang, Y. Lin, and H. Xin, "Dual-frequency electromagnetic cloaks enabled by LC-based metamaterial circuits," *Progress In Electromagnetics Research*, Vol. 119, 225–237, 2011.
12. Wang, B. and K.-M. Huang, "Spatial microwave power combining with anisotropic metamaterials," *Progress In Electromagnetics Research*, Vol. 114, 195–210, 2011.
13. Xu, S., L. Yang, L. Huang, and H. Chen, "Experimental measurement method to determine the permittivity of extra thin materials using resonant metamaterials," *Progress In Electromagnetics Research*, Vol. 120, 327–337, 2011.
14. Zhou, B., H. Li, X. Zou, and T.-J. Cui, "Broadband and high-gain planar Vivaldi antennas based on inhomogeneous anisotropic zero-index metamaterials," *Progress In Electromagnetics Research*, Vol. 120, 235–247, 2011.
15. Zhou, H., F. Ding, Y. Jin, and S. He, "Terahertz metamaterial modulators based on absorption," *Progress In Electromagnetics Research*, Vol. 119, 449–460, 2011.
16. Luukkonen, O., M. G. Silveirinha, A. B. Yakovlev, C. R. Simovski, I. S. Nefedov, and S. A. Tretyakov, "Effects of spatial dispersion on reflection from mushroom-type artificial impedance surfaces," *IEEE Trans. on Microwave Theory and Tech.*, Vol. 57, No. 11, 2692–2699, Nov. 2009.
17. Smith, D. R. and J. B. Pendry, "Homogenization of metamaterials by field averaging (invited paper)," *J. Opt. Soc. Am. B*, No. 23, 391–403, 2006.

18. Erentok, A. and R. W. Ziolkowski, "HFSS modeling of a dipole antenna enclosed in an epsilon-negative (ENG) metamaterial shell," *IEEE Antennas and Propagation Society International Symposium*, 22–25, Washigton DC, USA, Jul. 2005.
19. Caloz, C., C.-C. Chang, and T. Itoh, "Full-wave verification of the fundamental properties of left-handed materials in waveguide configurations," *J. Appl. Physics*, Vol. 90, No. 11, 5483–5486, 2001.
20. Gurel, L., O. Ergul, A. Unal, and T. Malas, "Fast and accurate analysis of large metamaterial structures using the multilevel fast multipole algorithm," *Progress In Electromagnetics Research*, Vol. 95, 179–198, 2009.
21. Jin, J., *The Finite Element Method in Electromagnetics*, John Wiley & Sons, New York, 1993.
22. Cevini, G., G. Oliveri, and M. Raffetto, "Further comments on the performances of finite element simulators for the solution of electromagnetic problems involving metamaterials," *Microw. Opt. Tech. Lett.*, Vol. 48, No. 12, 2524–2529, Dec. 2006.
23. Oliveri, G. and M. Raffetto, "A warning about metamaterials for users of frequency-domain numerical simulators," *IEEE Trans. on Antennas and Propag.*, Vol. 56, No. 3, 792–798, Mar. 2008.
24. Raffetto, M., "Ill posed waveguide discontinuity problem involving metamaterials with impedance boundary conditions on the two ports," *IET Proc. Sci. Measur. Tech.*, Vol. 1, No. 5, 221–239, Sept. 2007.
25. Oliveri, G. and M. Raffetto, "An assessment by a commercial software of the accuracy of electromagnetic finite element simulators in the presence of metamaterials," *The International Journal for Computation and Mathematics in Electrical and Electronic Engineering, COMPEL*, Vol. 27, No. 6, 1260–1272, 2008.
26. Oliveri, G. and M. Raffetto, "Accuracy of finite difference frequency domain methods in the presence of effective metamaterials," *Proceedings of the European Microwave Conference*, 27–31, Amsterdam, NL, Oct. 2008.
27. Bozza, G., G. Oliveri, and M. Raffetto, "Unusual ill-posed waveguide discontinuity problems: a comparison of frequency domain numerical methods," *9th International Workshop on Finite Elements for Microwave Engineering*, 8–9, Bonn, Germany, May 2008.
28. Clemens, M. and T. Weiland, "Discrete electromagnetism with the finite integration technique," *Progress In Electromagnetic*

Research, Vol. 32, 65–87, 2001.

29. Taflove, A. and S. C. Hagness, *Computational Electrodynamics: The Finite-difference Time-domain Method*, Artech House, Boston, 2000.
30. COMSOL, Inc., "COMSOL multiphysics 3.4," Jul. 2008, http://-www.comsol.com/.
31. Cevini, G., G. Oliveri, and M. Raffetto, "Performances of electromagnetic finite element simulators in the presence of three-dimensional double negative scatterers," *IET Proc. Microwav. Antennas Propag.*, Vol. 1, No. 3, 737–745, Jun. 2007.
32. Yee, K., "Numerical solution of inital boundary value problems involving Maxwell's equations in isotropic media," *IEEE Trans. on Antennas and Propag.*, Vol. 14, No. 3, 302–307, May 1966.
33. Clemens, M. and T. Weiland, "Numerical algorithms for the FDiTD and FDFD simulation of slowly varying electromagnetic fields," *International Journal of Numerical Modelling: Electronic Networks, Devices and Fields*, Vol. 12, No. 1–2, 3–22, 1999.
34. Champagne, N. J., J. G. Berryman, and H. M. Buettner, "FDFD: A 3D finite-difference frequency-domain code for electromagnetic induction tomography," *J. Comp. Physics*, Vol. 170, No. 2, 830–848, Jul. 2001.
35. Collin, R. E., *Foundations for Microwave Engineering*, McGraw-Hill, New York, 1992.
36. Caorsi, S., A. Massa, M. Pastorino, and A. Rosani, "Microwave medical imaging: Potentialities and limitations of a stochastic optimization technique," *IEEE Trans. on Microw. Theory and Tech.*, Vol. 52, No. 8, 1909–1916, Aug. 2004.
37. Oliveri, G., P. Rocca, and A. Massa, "A bayesian compressive sampling-based inversion for imaging sparse scatterers," *IEEE Trans. on Geosci. and Remote Sens.*, Vol. 49, No. 10, 3993–4006, Oct. 2011.
38. Oliveri, G., Y. Zhong, X. Chen, and A. Massa, "Multi-resolution subspace-based optimization method for inverse scattering," *J. Optical Soc. Am. A*, Vol. 40, No. 10, 2057–2069, Oct. 2011.
39. Rocca, P., M. Benedetti, M. Donelli, D. Franceschini, and A. Massa, "Evolutionary optimization as applied to inverse scattering problems," *Inverse Probl.*, Vol. 25, No. 12, 1–41, Dec. 2009.
40. Rocca, P., G. Oliveri, and A. Massa, "Differential evolution as applied to electromagnetics," *IEEE Antennas Propag. Mag.*, Vol. 53, No. 1, 38–49, Feb. 2011.